A Triple Active Bridge-Based Topology for Power Management in Green Hydrogen Production

Giuseppe Bossi, Alfonso Damiano
Department of Electrical and Electronic Engineering
University of Cagliari
Cagliari, Italy
giuseppe.bossi@unica.it, damiano@unica.it

***Abstract*—This paper proposes a DC/DC isolated conversion system based on the Triple-Active Bridge (TAB) topology for green hydrogen production. Specifically, the configuration involving a Photovoltaic (PV) power plant and an Energy Storage System (ESS) is investigated. The TAB's quasi-inherent decoupling feature and the use of Virtual Direct Power Control (VDPC) enable effective and independent management of power flows from the PV and ESS, even in the event that one of the sources fail and the ESS is charging due to PV overproduction. A simulation study on PLECS demonstrates the efficacy of the proposed configuration and shows that the system can manage the power flow of the TAB ports independently.**

***Index Terms*—Green hydrogen, DC/DC isolated converters, triple active bridge, energy management, photovoltaic, energy storage system, interleaved buck converter.**

I. Introduction

The utilisation of hydrogen as an essential energy carrier is now prevalent in several industrial sectors. The majority of hydrogen (65%) is utilised in the production of ammonia for fertilisers, while a significant proportion (25%) is allocated to the synthesis of methanol for pharmaceuticals, iron production (10%) and e-mobility, energy storage and power generation (1%). The present production of hydrogen typically involves steam methane reforming, also referred to as grey hydrogen, and coal gasification, also known as black/brown hydrogen. Nonetheless, in view of the mounting worldwide emphasis on attaining net-zero carbon emissions, the generation of hydrogen through electrolysis processes supplied by Renewable Energy Sources (RES), referred to as green hydrogen, appears to be a viable alternative [1], [2].

Commercial electrolyser stacks typically operate at low voltages and high currents [2]. Consequently, the utilisation of appropriate power electronics to regulate the voltage and current of the power source according to the stack's demands is imperative. A considerable number of interconnection schemes have been proposed in the existing literature: the majority of commercially available systems are grid-connected, while stand-alone systems are at the forefront of research activities in this field [3], [4]. This approach offers several advantages: firstly, the connection of the electrolyser to a DC power system, such as microgrids, allows for its direct interface with RES; secondly, the elimination of the line frequency transformer, inherited by the grid-connected interconnection topologies, improves the overall system efficiency and endows an enhanced scalability and flexibility. Consequently, the DC interconnection facilitates the development of improved converter topologies and the implementation of advanced control strategies for RES energy management [1]. In this regard, the isolated DC/DC converters represent a viable solution capable of efficiently interface an electrolyser stack. Among several topologies, the Dual-Active Bridge (DAB) represents one quoted solution, since its High-Frequency Transformer (HFT) provides galvanic isolation, reduces noise pollution, enhances electrical safety, and mitigates leakage currents issues [2], [3]. A DAB-based modular conversion system is considered a valuable approach to handle the high current values that characterise the working conditions of an Electrolysis System (ELS). In particular, the parallel connection of the DABs' input ports on a High-Voltage (HV) bus permits the power sharing and reduces current stresses, while the parallel connection of the output ports on a Low-Voltage (LV) bus, together with the transformer ratio, allows for current amplification to cope with the ELS requirements [2].

Nevertheless, the interconnection of multiple energy sources such as Photovoltaic (PV) power plants, Energy Storage Systems (ESS), Wind Turbines (WT) plants and the distribution grid to a single HV DC bus for supplying the ELS requires an improved number of properly controlled power electronic devices and an efficient energy management system [5]. Moreover, the interconnection of several conversion systems lead to complex instability phenomenon that needs to be properly addressed [6].

In this regard, the Multiport-Active Bridge (MAB) represents a viable alternative for interfacing multiple RES, characterised by different voltage operating conditions, and the distribution grid in one unique device. If a Triple-Active Bridge (TAB) is taken into account, a PV plant and an ESS can be interfaced and managed to feed the ELS, according to the diagram reported in Fig. 1. Notably, the power decoupling between TAB ports must be achieved to ensure efficient and independent power control [8]. In this configuration, the TAB is responsible for the power management and must be able to

This research was funded by the European Union – NextGenerationEU – PROMETH2eus project-ID RSH2A_000039 and the project "Ricerca di Sistema Elettrico - Accordo di Programma Ministero dell'Ambiente e della Sicurezza Energetica -ENEA Piano Triennale di Realizzazione 2022-2024, Progetto Integrato Tecnologie dell'idrogeno", CUP: I53C22003020001.

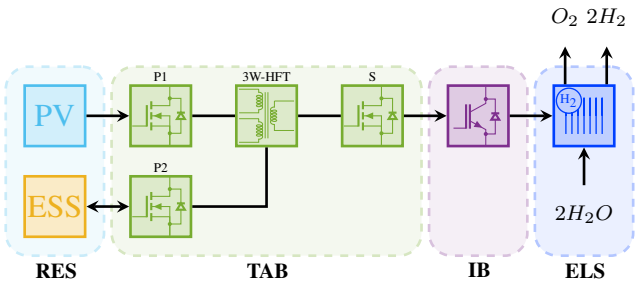

Fig. 1. The proposed TAB-based conversion system for electrolysers.

cope with any operating conditions. In this regard, the Virtual Direct Power Control Scheme (VDPC) provides an efficient power management with high-performance dynamics and is able to handle situations such as: the PV system is set as the main source and, in conditions of overproduction, it feeds the ELS and charges the ESS; the ELS requires a higher power supply than the PV production can provide and hence the ESS compensates for the difference; a fault may occur that requires the ELS power to transition quickly from one source to another [7].

An Interleaved Buck (IB) converter is placed to condition the TAB output to meet the voltage and current requirements of the ELS. Compared to more complex HV systems, the stability analysis of two conversion devices connected in series, such as a TAB and an IB, is simpler and more straightforward approaches can be employed [11].

This paper investigates the TAB-based DC/DC isolated conversion system shown in Fig. 1 for an effective power management of a PV power plant and an ESS to feed an ELS for green hydrogen production. The paper is structured as follows; Section II presents the DC/DC conversion system topology, the design assumption, the VDPC control strategy and the IB current control; Section III shows the simulation study results and in Section IV the conclusion remarks are reported.

II. DC/DC Isolated Conversion System

The proposed TAB-based DC/DC isolated conversion system is shown in Fig. 2. The TAB presents two input ports: the first one, indicated as P1, is interfaced with the PV plant by means of its own DC/DC power conditioning system and is constituted by a full bridge and a DC-link capacitor C_{P1}; the second input full bridge, indicated as P2, presents the capacitor DC-link C_{P2} and interfaces the ESS. On the other side, the output port S is a full bridge characterised by the DC-link capacitor C_S and is connected to the IB toward the ELS. The magnetic tank ensures the power coupling of P1 and P2 toward S. It is composed of the Three-Winding High-Frequency Transformer (3W-HFT) and the leakage inductances L_{P1} and L_{P2}, positioned on P1 and P2, respectively. In particular, the 3W-HFT ensures the galvanic isolation between the power sources and the ELS. In addition, the transformation ratios n_{P1} and n_{P2} defined as V''/V' allows for voltage scaling toward the ELS requirements. Concurrently, the external inductors L_{P1} and L_{P2} directly participate to the TAB power control. The most common modulation technique for the TAB is known as Single Phase Shift (SPS). Its main advantages lie in simplicity and in the achievement of soft switching conditions in well-defined operating ranges. Conversely, its main disadvantages consist in the presence of high peak currents on the HFT and flow-back currents on the DC sides. Furthermore, the achievement of soft switching conditions and the zero re-circulation power inside the magnetic tank constrain the TAB working conditions in terms of voltage and power set-points. In order to overcome the aforementioned problems and improve the performance of TAB, advanced modulation techniques such as Double-Phase Shift (DPS) and Triple Phase Shift (TPS) have been proposed [9], [10].

The IB conversion system is composed of four buck converters connected in parallel. The legs of the IB modulate with a phase shift of $\pi/2$ between each other, and their duty cycles are used to control the current I_{ELS}. In this way, the current ripple is mitigated at the node A in Fig. 2, ensuring power quality for the ELS.

The stability of the TAB and the IB series connection is always verified concerning the impedance-based stability criterion [11].

A. TAB Control Strategy

The TAB control must ensure independent and effective power management of both PV and ESS toward the ELS. Moreover, it must contemplate the charging scenario of the ESS in the case PV's overproduction. Firstly, the power decoupling between P1 and P2 must be guaranteed by means of a decoupling strategy. The inherent decoupling method is employed, in which the port S is assumed as the master port i.e. a port of the TAB where the external leakage inductance is not placed. In this way, a theoretical decoupling is achieved between P1 and P2. Nevertheless, if the 3W-HFT exhibits an internal leakage inductance sufficiently small to be less than 5 % of L_{P1} and L_{P2} transposed on the master port, a *quasi*-inherent decoupling is achieved and the ports are considered independent from each other [8].

The external leakage inductances L_{P1} and L_{P2} have been designed concerning the TAB power expression of (1) [12]

$$P_{PkS} = \frac{V_{Pk} V_S D_{Pk}(1 - |D_{Pk}|)}{2 L_{Pk} f_{sw} n_{Pk}}; \qquad k = 1, 2, \tag{1}$$

where V_{Pk} is the voltage on either the P1 or P2 ports, D_{Pk} is the normalised phase shift defined as γ_{Pk}/π, n_{Pk} is the turn ratio of the transformer between port P_k and S and f_{sw} is the TAB switching frequency. Assuming a maximum value $D_{Pk} = 0.2$ for ensuring to work into the linear interval of the power characteristic, the maximum power P^*_{PkS} is evaluated in (2)

$$P^*_{PkS} = \frac{2 V_{Pk} V_S}{25 L^*_{Pk} f_{sw} n_{Pk}}; \qquad k = 1, 2, \tag{2}$$

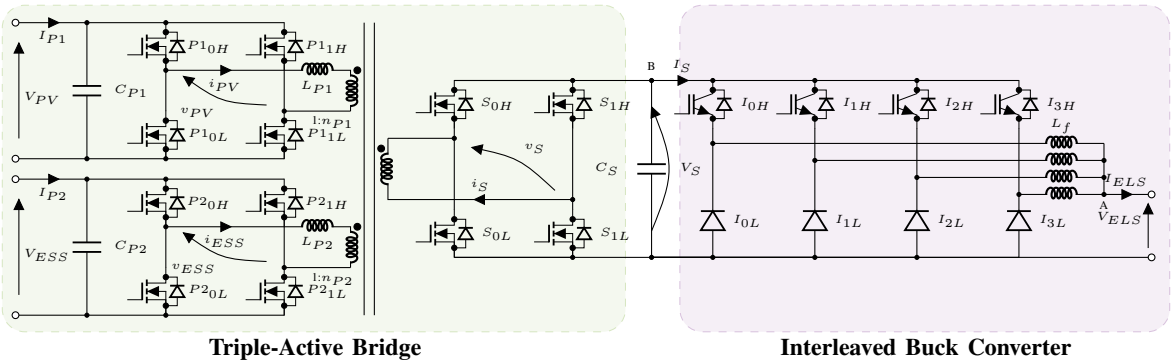

Fig. 2. The proposed TAB-based conversion system topology.

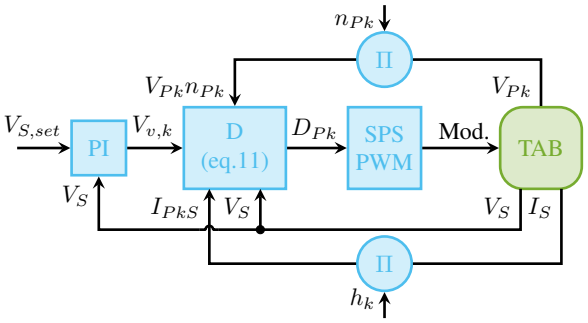

Fig. 3. VDPC applied for the TAB port P_k (k=1,2) toward S.

from which the design value L^*_{Pk} is determined as reported in (3)

$$L^*_{Pk} = \frac{2V_{Pk}V_S}{25P^*_{Pk}f_{sw}n_{Pk}}; \qquad k=1,2,. \tag{3}$$

The design is validated if the quasi-inherent decoupling is verified i.e. the ratio $\alpha = L_{S,int}/L_{S,Pk}$, where $L_{S,Pk}$ is L_{Pk} transposed on the S side, is below 5 %.

The SPS control strategy is implemented resorting to the VDPC shown in Fig. 3 [7]. The control strategy allows for controlling the power share between ESS and PV by varying the power gain h according to the power balance of the system reported in (4)

$$P_{ELS} = P_{PV} + P_{ESS}, \tag{4}$$

and by exploiting the balance concerning voltage and currents, (4) becomes (5).

$$I_S = \left(\frac{V_{PV}}{V_S}I_{P1}\right)h_1 + \left(\frac{V_{ESS}}{V_S}I_{P2}\right)h_2; \quad h_1 + h_2 = 1 \tag{5}$$

By assuming that V_{PV} and V_{ESS} are constant, also V_S must be set in order to achieve the desired power share by ports' current control. In this way, the power balance is ensured by the current balance in the node B of Fig. 2, hence making C_S the DC power node of the TAB converter.

Therefore, the control algorithm, distinguished for ports P1 and P2, must satisfy the required $I_S h_k$ and set the output voltage V_S. To achieve this goal, the TAB output impedance is controlled. The TAB power of (1) can be transposed on the port S assuming the form of (6)

$$P_{PkS} = \frac{V_{Pk}V_S n_{Pk}D_{Pk}(1-|D_{Pk}|)}{2L_{S,Pk}f_{sw}}; \qquad k=1,2. \tag{6}$$

Assuming that $L_{S,P1}$=$L_{S,P2}$=L_S, equation (6) can be unified concerning the term $L_S f_{sw}$, as reported in (7)

$$p_{PkS} = \frac{V_{Pk}V_S n_{Pk}D_{Pk}(1-|D_{Pk}|)}{2}; \qquad k=1,2. \tag{7}$$

The virtual power reference $p_{v,k}$ (k=1,2) is defined in (8)

$$p_{v,k} = |V_{v,k}|I_{S,set}h_k; \qquad k=1,2, \tag{8}$$

where the desired virtual output voltage $V_{v,k}$ represents the control variable given by the PI controller. $V_{v,k}$ is a parameter that represents the correction to achieve the desired output impedance. Therefore, the control task is to achieve the relationship of (9)

$$\frac{V_{S,set}}{I_{S,set}} = \frac{V_S}{I_S}. \tag{9}$$

By isolating $I_{S,set}$ and integrating (9) into (8), the unified power reference is given in (10)

$$p_{v,k} = \frac{|V_{v,k}|V_{S,set}I_S h_k}{V_S}. \tag{10}$$

Imposing $p_{PkS} = p_{v,k}$ and solving for D_{Pk} (k=1,2), the phase shift between port P_k and S is found (11)

$$D_{Pk} = \begin{cases} \frac{1}{2} - \sqrt{\frac{1}{4} - \frac{2V_v V_{S,set}I_S h_k}{V_{Pk}V_S^2 n_{Pk}}}; & i_S h_k \geq 0 \\ -\frac{1}{2} + \sqrt{\frac{1}{4} + \frac{2V_v V_{S,set}I_S h_k}{V_{Pk}V_S^2 n_{Pk}}}. & i_S h_k < 0 \end{cases} \tag{11}$$

Being $I_S h_1$ of the PV plant always greater than 0, $I_S h_2$ can assume negative values since the ESS contemplates also the charging condition. Notably, the sign of $I_S h_2$ depends on h_2, since I_S is always positive toward ELS. However, the balance of (5) must be always ensured.

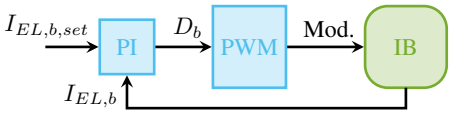

Fig. 4. Current control of each IB buck stage.

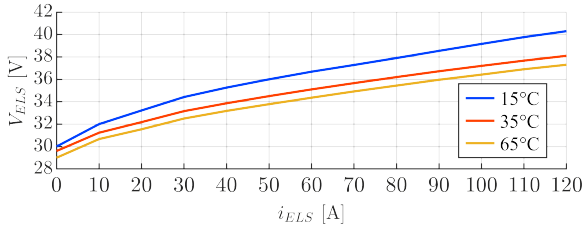

Fig. 5. $V_{ELS}vs.i_{ELS}$ of the ELS stack considered in the simulations.

B. IB Control Strategy

The IB conversion system supplies I_{ELS} to the ELS ensuring a good power quality. To perform this task, four different PI current loops control each buck stage. Hence, I_{ELS} is divided symmetrically on each buck as reported in (12)

$$I_{ELS} = 4I_{ELS,b}. \tag{12}$$

The control scheme of each stage is shown in Fig. 4.

III. Simulation Results

A simulation study of the proposed TAB-based DC/DC isolated conversion system for an ELS has been carried out on PLECS. A commercial advanced alkaline water stack has been considered and its characteristic evolutions are reported in Fig. 5 for the operative temperatures of 15 °C, 35 °C and 65 °C. The stack has a rated current of 120 A, at which 1 Nm^3/h of H_2 is produced, and is composed by 22 round cells of 300 cm^2 connected in series. It can operate into the pressure span of 4 bar to 25 bar with a rated temperature of 65 °C [13].

The leakage inductors L_{P1} and L_{P2} has been designed to fulfil the ELS power requirement and the inherent decoupling between ports P1 and P2. The system parameters are reported in Table I. The design contemplates the supply of 5 kW peak power, achieved when the ELS works at 15°C and 120 A. In order to take into account every working condition, both PV and ESS must be able at least to supply the entire ELS power. In particular, the PV must ensure an overproduction condition to charge the ESS. The L_{P1} and L_{P2} are sized applying (3) considering the parameters of Table I. Hence, the design outcomes an L_{P1} and L_{P2} values of 600 μH and 150 μH, respectively. Given that $L_{S,int}$ is equal to 1.5 μH, the α parameter is established at 4 % and hence the quasi-inherent decoupling of the TAB ports P1 and P2 is achieved.

Since it is convenient for the ELS to works in the linear region of its characteristics, i.e. between 30 A and 120 A as shown in Fig. 5, the IB is always in continuous conduction mode, meaning that, during normal operations, the current of every buck stage never goes to zero due to the ripple amplitude.

TABLE I
DC/DC Conversion System Datasheet.

Parameters	Values
PV plant voltage V_{PV}	600 V
ESS voltage V_{ESS}	300 V
ELS voltage setpoint $V_{S,set}$	150 V
Switching Frequency f_{sw}	10 kHz
DC-Link Capacitors C_{P1}, C_{P2}, C_S	520 μF
Transf. Magnetising Inductance L_m	2m H
Transf. Leakage Inductance $L_{S,int}$	1.5 μH
Turn Ration n_{P1}	0.25
Turn Ration n_{P2}	0.5
External Leakage Inductance L_{P1}	600 μH
External Leakage Inductance L_{P2}	150 μH
Interleaved Filter Inductance L_f	2.5 mH
Dead time $t_{deadband}$	250 ns

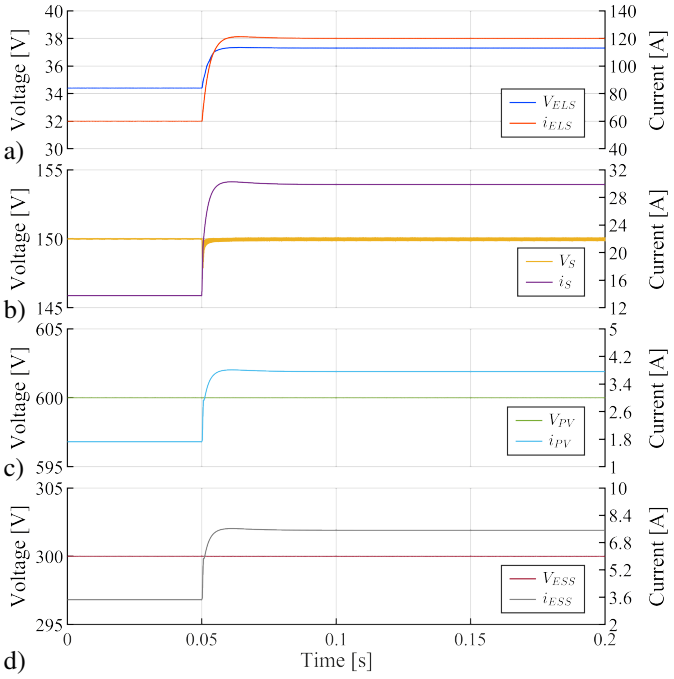

Fig. 6. Voltage and current evolutions during a step-load between 60A and 120A while the PV feeds 50% of the ELS power: a)V_{ELS} and i_{ELS}: b) V_S and i_S; c) V_{PV} and i_{PV}; d) V_{ESS} and i_{ESS}.

The system thus designed is simulated and the results are shown from Fig. 6 to Fig. 10. The system is started up and an initial production of 60 A is established at the rated temperature of 65 °C. In these conditions, 2.1 kW are supplied to the ELS, and it is initially assumed that the PV supplies 50 % of the power. Afterwards, the ELS production changes to its rated value of 120 A and 4.5 kW are supplied. The Fig. 6 shows the transition, demonstrating good dynamic results of the DC/DC system in controlling both I_{ELS} and V_S. The Fig. 7 shows the normalised buck currents $I_{ELS,b}$ compared to the normalised I_{ELS}, highlighting how the buck stages interact and mitigate the current ripple of I_{ELS}, thus endowing good power quality.

Afterwards, the demand for hydrogen drops and the production is established again at 60 A. Under the hypothesis that the ESS is discharged and the power balance is assured, the PV power share changes from 50 % to 80 %. The transition

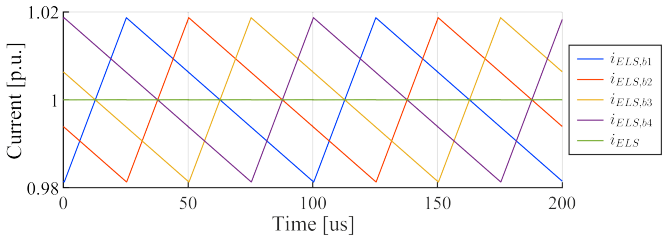

Fig. 7. IB currents towards the ELS.

is assumed to happen as a ramp with a slope of 10 $\%/s$, and the evolution is shown in Fig. 8a and Fig. 8b. In particular, from Fig. 8a it can be seen the power regulation, while Fig. 8b highlights that a small perturbation on both V_S and I_{ELS} is registered during the transition, thus exhibiting a good stability of the system even if the power share changes. The Fig. 8c and Fig. 8d show the voltage and current evolutions on the transformer at 50 % of power share, highlighting that, as expected, the phase shifts D_{P1} and D_{P2} presents the same value. Conversely, Fig. 8e and Fig. 8f show that, while the PV is producing the 80 % of the power, the phase shift D_{P1} is higher than D_{P2}.

By considering a PV plant overproduction of 30 %, the ESS is placed under charge. If a starting condition of 50 % power share between the PV and ESS is considered, a ramp transition with a rate of 10 $\%/s$ is applied to reach 130 % i.e. the PV supplies the 100 % of the ELS requirements plus 30 % for charging the ESS. The system evolution is reported in Fig. 9. It is shown that the power of the ESS reverted without any relevant perturbation on the ELS, thus demonstrating the effectiveness of the ESS charging mode.

If a fault on the PV plant happens, the current is shut down immediately and it is imperative that the ESS takes action to supply the power to the ELS. Starting from a condition in which the PV produced 50 % of the power, the Fig. 10 shows the system evolution while the PV production goes to 0 %. It shows good dynamics, demonstrating the resilience of the VDPC. As expected, besides D_{P1} is zero, a small power of 80 W flows from P2 to P1. Since the power flowing from the ESS toward the ELS is of 2.2 kW, their ratio is of about 4 %, which represents the coupling amount forecasted by α. This proves the achievement of the quasi-inherent decoupling between P1 and P2 as forecasted in the design stage.

IV. Conclusion

This paper proposes a Triple-Active Bridge-based DC/DC isolated conversion system to supply a green hydrogen power plant from Renewable Energy Sources. The system ensures an effective power management of the PV power plant and the ESS connected to the TAB inputs. A proper design procedure is proposed for the external leakage inductances to fulfil both the rated power of the electrolysis system and the quasi-inherent power decoupling between the PV and the ESS. The TAB output is conditioned by an interleaved buck converter to meet the voltage and current requirements of the ELS. The simulation study performed using PLECS demonstrates the feasibility of the proposed configuration. In particular, the use of a robust Virtual Direct Power Control ensures power balance even when the ESS is being charged from the PV plant or if one of the two energy sources fails. Moreover, the interleaved buck system guarantees good power quality by mitigating the current ripple toward the ELS.

Acknowledgment

This research was funded by the European Union – NextGenerationEU – PROMETH2eus project-ID RSH2A_000039 and the project "Ricerca di Sistema Elettrico - Accordo di Programma Ministero dell'Ambiente e della Sicurezza Energetica -ENEA Piano Triennale di Realizzazione 2022-2024, Progetto Integrato Tecnologie dell'idrogeno", CUP: I53C22003020001.

References

[1] A. Hassan, O. Abdel-Rahim, M. Bajaj, and I. Zaitsev, "Power electronics for green hydrogen generation with focus on methods, topologies, and comparative analysis," *Scientific Reports (Nature Publisher Group)*, vol. 14, no. 1, p. 24767, 2024.

[2] G. Rego, J. Rocha, J. A. Faria, J. L. Afonso, and V. Monteiro, "A Review of Hydrogen Production Methods and Power Electronics Converter Topologies for Green Hydrogen Applications," *Energies*, vol. 17, no. 22, p. 5579, Jan. 2024.

[3] H. Renaudineau, A. M. Llor, R. Cortés D., C. A. Rojas, C. Restrepo, and S. Kouro, "Photovoltaic Green Hydrogen Challenges and Opportunities: A Power Electronics Perspective," *IEEE Industrial Electronics Magazine*, vol. 16, no. 1, pp. 31–41, Mar. 2022.

[4] M. B. El Kattel, P. P. Praça, R. Mayer, C. d. C. Lucio Berrehil el Kattel, R. P. T. Bascopé, F. L. M. Antunes, and B. de Jesus Cardoso Filho, "Overview of Main Electrolyzer Technologies and Power Electronic Converter Topologies for Enabling Hydrogen Production Through Water Electrolysis," *International Journal of Circuit Theory and Applications*, vol. n/a, no. n/a.

[5] N. Hou, L. Ding, P. Gunawardena, T. Wang, Y. Zhang, and Y. W. Li, "A Partial Power Processing Structure Embedding Renewable Energy Source and Energy Storage Element for Islanded DC Microgrid," *IEEE Transactions on Power Electronics*, vol. 38, no. 3, pp. 4027–4039, Mar. 2023.

[6] X. Zhang, X. Ruan, and C. K. Tse, "Impedance-Based Local Stability Criterion for DC Distributed Power Systems," *IEEE Transactions on Circuits and Systems I: Regular Papers*, vol. 62, no. 3, pp. 916–925, Mar. 2015.

[7] W. Song, N. Hou, and M. Wu, "Virtual Direct Power Control Scheme of Dual Active Bridge DC–DC Converters for Fast Dynamic Response," *IEEE Transactions on Power Electronics*, vol. 33, no. 2, pp. 1750–1759, Feb. 2018.

[8] G. Bossi, N. Campagna, M. Boi, R. Miceli, and A. Damiano, "An Inherent Decoupled Triple-Active Bridge Converter for All-Electric Aircraft DC Power Systems," *Energies*, vol. 17, no. 24, p. 6368, Jan. 2024.

[9] H. Tao, J. L. Duarte, and M. A. M. Hendrix, "Three-Port Triple-Half-Bridge Bidirectional Converter With Zero-Voltage Switching," *IEEE Transactions on Power Electronics*, vol. 23, no. 2, pp. 782–792, Mar. 2008.

[10] G. Bossi, C. Song, A. Sangwongwanich, F. Blaabjerg, and A. Damiano, "A Harmonic-Based Triple Phase Shift Modulation Strategy for a Dual Active Bridge Converter in an All Electric Aircraft Application," in *2024 International Symposium on Power Electronics, Electrical Drives, Automation and Motion (SPEEDAM)*, Jun. 2024, pp. 1117–1123.

[11] J. Sun, "Impedance-Based Stability Criterion for Grid-Connected Inverters," *IEEE Transactions on Power Electronics*, vol. 26, no. 11, pp. 3075–3078, Nov. 2011.

[12] G. Bossi, C. Buccella, C. Cecati, A. Damiano, A. Floris, and F. Simonetti, "A Converter Topology for Auxiliary Power System of an All Electric Aircraft," in *2023 IEEE Energy Conversion Congress and Exposition (ECCE)*, Oct. 2023, pp. 1605–1612.

[13] A. Ursúa and P. Sanchis, "Static–dynamic modelling of the electrical behaviour of a commercial advanced alkaline water electrolyser," *International Journal of Hydrogen Energy*, vol. 37, no. 24, pp. 18 598–18 614, Dec. 2012.

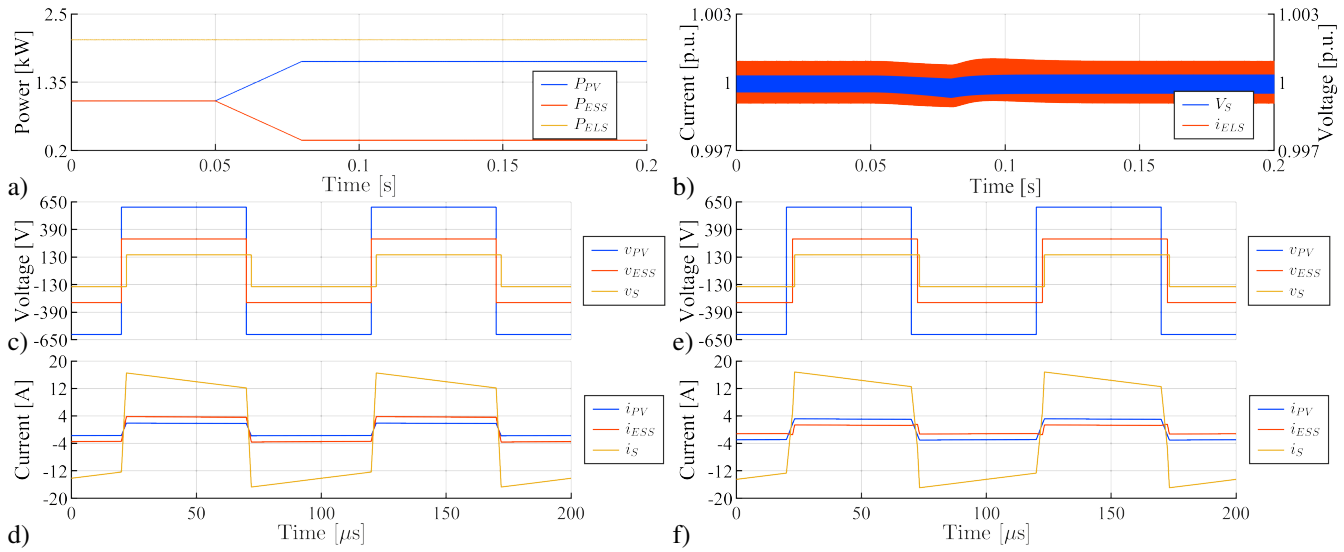

Fig. 8. Voltage and current evolutions while the PV feeds changes from 50% to 80% while 60A to the ELS are supplied: a)P_{ELS}, P_{PV} and P_{ESS}; b) V_S and i_{ELS} in normalised over their set values; c) v_{PV}, v_{ESS} and v_S while PV feeds is at 50%; d) i_{PV}, i_{ESS} and i_S while PV feeds is at 50%; e) v_{PV}, v_{ESS} and v_S while PV feeds is at 80%; f) i_{PV}, i_{ESS} and i_S while PV feeds is at 80%.

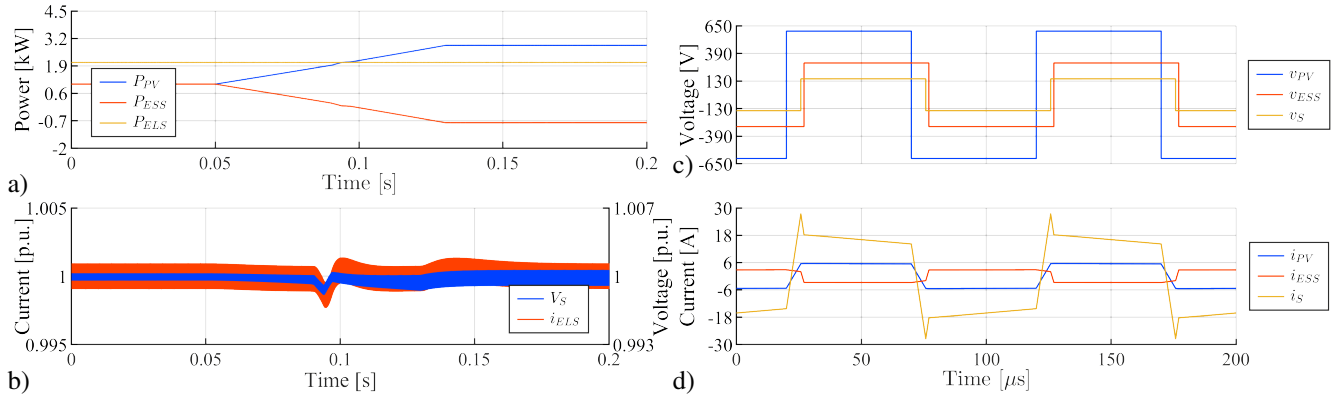

Fig. 9. Voltage and current evolutions while the PV feeds changes from 50% to 130% for ESS charging while 60A to the ELS are supplied: a)P_{ELS}, P_{PV} and P_{ESS}; b) V_S and i_{ELS} normalised over their set values; c) v_{ESS}, v_{PV} and v_S while the PV power share is at 130%; d) i_{PV}, i_{ESS} and i_S while the PV power share is at 130%.

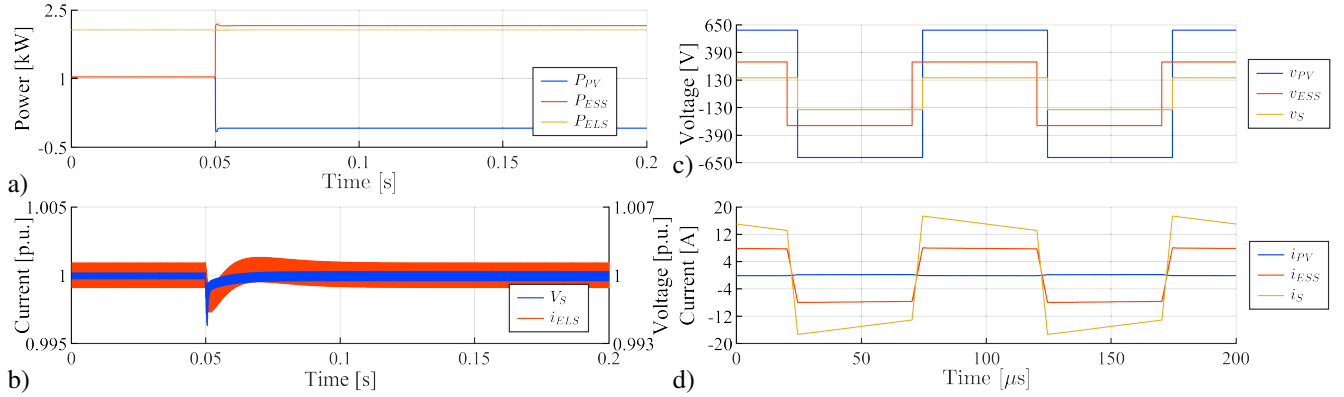

Fig. 10. Voltage and current evolutions while the PV feeds changes from 50% to 0% while 60A to the ELS are supplied: a)P_{ELS}, P_{PV} and P_{ESS}; b) V_S and i_{ELS} in normalised over their set values; c) v_{PV}, v_{ESS} and v_S while PV feeds is at 0%; d) i_{PV}, i_{ESS} and i_S while PV feeds is at 0%.